ELSEVIER

International Journal of Solids and Structures 41 (2004) 5663–5675

INTERNATIONAL JOURNAL OF SOLIDS and STRUCTURES

www.elsevier.com/locate/ijsolstr

An inclined Zener–Stroh crack near a free surface

J.F. Zhao, Z.M. Xiao *

School of Mechanical and Production Engineering, Nanyang Technological University, Singapore

Received 9 October 2003; received in revised form 23 April 2004
Available online 5 June 2004

Abstract

Machining of a material surface often produces large shear stress beneath the free surface, which causes dislocations piled up along a slip plane near the surface until those dislocations are stopped by an obstacle and nucleates a microcrack at the subsurface. The nucleated microcrack due to dislocation pile-up is called a Zener–Stroh crack which has many properties different to a conventional Griffith crack. In this paper, the physical mechanism of such microcrack initiation has been discussed. Stress investigation on the problem of a subsurface Zener–Stroh crack inclined to the free surface of a material has been carried out. By using the stress solution of a single dislocation in a half plane as the Green's function, the microcrack is simulated with distributed dislocations along the crack line. A set of singular integral equations are then formulated and solved with numerical method. Results show that the influence of the free surface on the stress intensity factors (SIFs) of the crack and the critical crack length greatly depends on the slant angle. The free surface also brings intrinsic coupling phenomenon for the Mode I and Mode II SIFs. As a result this coupling effect changes the fracture toughness of the material.

Keywords: Inclined subsurface Zener–Stroh crack; Stress intensity factor; Dislocation

1. Introduction

Surface machining process produces shear stress beneath the free surface of a material. Such induced shear stress can be fairly large near the free surface. In many cases, this shear stress moves dislocations along a slip plane parallel to the surface until the dislocations being stopped by an obstacle, such as a grain boundary. When the piled-up dislocations reach a large amount, one way to release the high strain energy is to nucleate a microcrack, as illustrated in Fig. 1. This type of subsurface microcrack was observed in the grinding process of ceramics material recently (Zhang et al., 2003). This dislocation-based subsurface crack is very different to the surface crack appearing in machining process or other rolling contact, which is generally a interacting procedure between lubricating fluid and edge cracks (Bower, 1988; Hsia and Xu, 1996; Xu and Hsia, 1997). In fact, this microcrack nucleation mechanism was early developed by Zener

* Corresponding author. Tel.: +65-679-04726; fax: +65-679-11859/21859.
E-mail address: mzxiao@ntu.edu.sg (Z.M. Xiao).

0020-7683/$ - see front matter © 2004 Elsevier Ltd. All rights reserved.
doi:10.1016/j.ijsolstr.2004.04.040

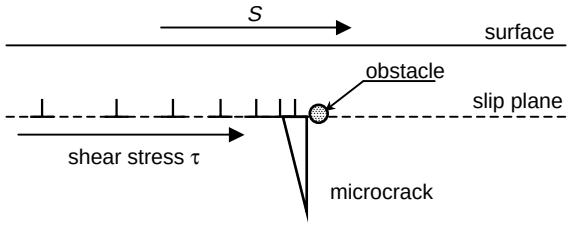

Fig. 1. Nucleation of a subsurface microcrack.

(1948), who first reasoned that piled-up dislocations can nucleate a microcrack. Later, Stroh's (1954, 1955) independent analysis gave the amount of dislocations needed for such nucleation in the absence/presence of a slip plane. This type of microcracks was named Zener–Stroh crack by following researchers (Weertman, 1986). There are also other similar nucleation mechanisms on such microcracks induced by dislocation pile-up (Cottrell, 1958; Kikuchi et al., 1981).

Different to the famous Griffith crack which has a symmetric stress field, a Zener–Stroh crack in a homogeneous material has an antisymmetric stress field. The total crack opening displacement in such a crack is not zero. With these peculiar properties, the microcrack propagates faster than Griffith crack in cyclic stress field, which often encountered in machining process (Weertman, 1986).

Two important parameters characterizing a Zener–Stroh crack are the stress intensity factor (SIF) and the critical crack length. For a crack in a homogeneous material loaded by both net dislocations (with net Burgers vector b^{T}) and external stress σ, the energy stored in the system as a function of crack length is schematically depicted in Fig. 2. The SIF K_{ZS} due to the Zener–Stroh mechanism under the loading of net dislocations b^{T} is given by

$$K_{\mathrm{ZS}} = \frac{\mu b^{\mathrm{T}}}{2(1-\nu)\sqrt{\pi a}}, \tag{1}$$

where a is the half crack length, μ is the shear modulus, and ν is the Poisson's ratio. At the same time the SIF K_{G} due to the Griffith mechanism with a stress loading σ is given by

$$K_{\mathrm{G}} = \sigma\sqrt{\pi a}. \tag{2}$$

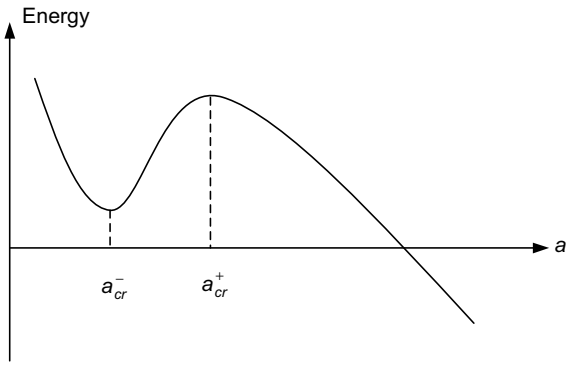

Fig. 2. Critical crack length of Griffith–Zener–Stroh crack.

As a result, the critical crack length a_{cr} for a crack controlled by these two mechanisms is determined by

$$(K_{ZS} + K_G)^2 = \left(\frac{Gb^T}{\sqrt{2\pi a_{cr}}} + \sigma\sqrt{\pi a_{cr}} \right)^2 = K_C^2. \tag{3}$$

The above second order equation gives two solutions for a_{cr}: from Fig. 2, the smaller a_{cr}^- is under Zener–Stroh crack mechanism and is energywise stable; the larger a_{cr}^+ corresponds to the Griffith crack mechanism and is energywise unstable. The smaller value a_{cr}^- controlled by Zener–Stroh mechanism gives the original size of the crack; while the larger value a_{cr}^+ controlled by Griffith crack mechanism predicts the moment of unstable crack propagation.

In recent years, more research work on Zener–Stroh (Z-S) crack can be found in open literature, such as Cherepanov (1994) and Fan (1994) on interface Zener–Stroh crack, Xiao and Fan (1996) on a Z-S crack at a tip of a rigid line inhomogeneity and near an interface (Fan and Xiao, 1997). They studied the required dislocation amounts to form a Z-S crack, the critical crack length, the stress field and SIFs in the corresponding structure configurations. However, the problem for a general subsurface Zener–Stroh crack is still waiting to be investigated, while the case for a Griffith crack in such a geometric configuration has been studied by various researchers (Hills and Comninou, 1985; Hearle and Johnson, 1985; Nowell and Hills, 1987). Different to the situation of an interface crack where the interface works as an obstacle to nucleate the crack, a subsurface crack is nucleated in a new environment with the aid of very large shear stress due to surface treatment. In the present paper, we start with the discussion on the factors influencing the subsurface microcrack nucleation based on the famous Zener–Stroh mechanism. Then the physical problem for a general subsurface Z-S crack with a slanting angle to the surface is formulated. The effect of the free surface on the Mode I and Mode II SIFs of the crack, as well as the critical crack length has been analyzed. The influence of other parameters, such as the depth and slant angle of the crack, on the fracture behavior of the crack is also studied and discussed.

2. Crack initiation mechanism

Refer to Fig. 1, as discussed in Section 1, dislocations are moved along a slip plane by the shear force due to surface machining. The piled-up dislocations create a singular stress field which pulls the material open. A micro-Zener–Stroh crack is thus nucleated. For the current configuration in Fig. 1, the force on a single dislocation comes from three sources: the driving force F_τ produced by the shear stress, the interaction force F_d from other dislocations and the force F_g from the grain boundary.

The force on the dislocation induced by the shear force can be calculated with Peach–Koehler formulae (Dundurs, 1969):

$$F_\tau = b_y \tau, \tag{4}$$

where b_y is the component of Burgers vectors of a dislocation, and τ is the shear stress which depends on the manufacturing technology and the distance to the surface. For instance, polishing on the surface induces a shear stress (Minowa and Sumino, 1992),

$$\tau = \frac{P}{4\pi R^2} \left[-(1+2\nu) + 2(1+\nu)\frac{h}{(R^2+h^2)^{1/2}} - 3\frac{h^3}{(R^2+h^2)^{3/2}} \right], \tag{5}$$

where P is the normal scratching force and R is the radius of contact circle. F_τ generally holds a large value at a small depth from the above equation and is the propelling force to pile the dislocations at the grain boundary.

The interaction force F_d has the form of

$$F_d = \sum_i \left(\frac{K\mu b_y^2}{2\pi(1-\nu)} \right) \frac{1}{L_i}, \tag{6}$$

where μ is the shear modulus and K is a function to be given in detail later, and L_i is the distance from the considered dislocation to the ith dislocation. Because these dislocations locate in the same direction, the interaction force is repulsive and resists the pile-up.

The force F_g due to grain boundary is complicated and difficult to quantify. But the force from the grain boundary should be related to the material properties, the shape and the size of the grain and distance from the grain.

After the dislocation is moved, it reaches a equilibrium position and the total force on it is reduced to zero,

$$F_\tau - F_d - F_g = 0. \tag{7}$$

With the increasing piled-up dislocations, a very large interaction force F_d is produced to cancel the force F_τ from the shear stress to move more dislocations to the grain boundary. If the expression of F_g is found, the above equation can be used to evaluate the number of piled-up dislocations. According to Cherepanov's (1994) analysis, when the number of piled up dislocations reach a certain value, a micro-Z-S crack will be formed. The nucleated crack is loaded with a displacement loading b^T (the total Burgers vectors of the piled-up dislocations), provided there is no other stress tractions on the crack. The crack tip where the dislocations enter the crack is called the blunt tip, while the other crack tip is called the sharp tip. Crack can propagate from the sharp tip only.

3. Formulation on an inclined subsurface Zener–Stroh crack

In this section, stress investigation is to be done on a micro-Z-S crack initiated inclining to the free surface with a slant angle θ, as shown in Fig. 3. The crack length is denoted as $2a$, and the distance from the center of the crack to the surface is d. The global coordinate system x–y sits on the position as given in the figure. To simulate the microcrack with distributed dislocations, we need the stress solution for a single

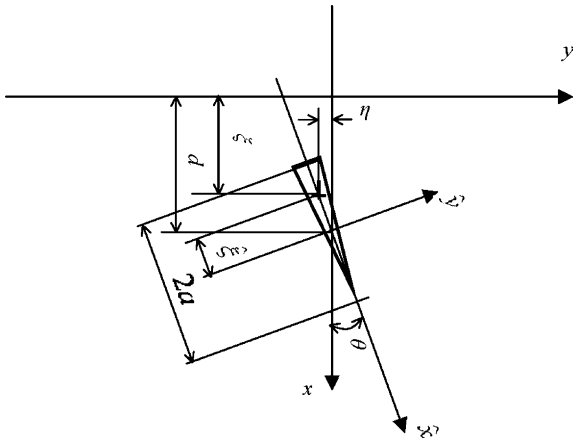

Fig. 3. An inclined Zener–Stroh crack near the free surface of a material.

dislocation in a half plane as the Green function. The stress field due to a single dislocation located at a point (ξ,η) with Burgers vector components b_x and b_y in a half plane is given by (Hills et al., 1996)

$$\sigma_{xx}(x,y)=\frac{2\mu}{\pi(\kappa+1)}[b_x(\xi)G_{xxx}(x;y;\xi,\eta)+b_y(\xi)G_{yxx}(x;y;\xi,\eta)], \tag{8a}$$

$$\sigma_{yy}(x,y)=\frac{2\mu}{\pi(\kappa+1)}[b_x(\xi)G_{xyy}(x;y;\xi,\eta)+b_y(\xi)G_{yyy}(x;y;\xi,\eta)], \tag{8b}$$

$$\sigma_{xy}(x,y)=\frac{2\mu}{\pi(\kappa+1)}[b_x(\xi)G_{xxy}(x;y;\xi,\eta)+b_y(\xi)G_{yxy}(x;y;\xi,\eta)], \tag{8c}$$

where G are the influence functions and κ is the Kolosov's constant. In order to facilitate the expression of the traction free condition along the crack line, a new local coordinate system $(\hat{x},\hat{y})$ is introduced in Fig. 3. The origin of the system is the center of the crack, the angle between the new and old x-axes is the crack slanting angle θ. The stress field due to the same dislocation in the new local coordinate system could be written in

$$\begin{Bmatrix}\sigma_{\hat{y}\hat{y}}(\hat{x},\hat{y})\\ \sigma_{\hat{x}\hat{y}}(\hat{x},\hat{y})\end{Bmatrix}=\frac{2\mu}{\pi(\kappa+1)}\begin{bmatrix}G_{\hat{x}\hat{y}\hat{y}}(\hat{x},\hat{y};\hat{\xi}) & G_{\hat{y}\hat{y}\hat{y}}(\hat{x},\hat{y};\hat{\xi})\\ G_{\hat{x}\hat{x}\hat{y}}(\hat{x},\hat{y};\hat{\xi}) & G_{\hat{y}\hat{x}\hat{y}}(\hat{x},\hat{y};\hat{\xi})\end{bmatrix}\begin{Bmatrix}b_{\hat{x}}(\hat{\xi})\\ b_{\hat{y}}(\hat{\xi})\end{Bmatrix}. \tag{9}$$

The detailed expressions for the transformed and original influence functions G_{ijk} are given in Appendix A. Now we assume the crack is simulated by distributed dislocations along the crack line, with $B_{\hat{x}}(\hat{\xi})$ and $B_{\hat{y}}(\hat{\xi})$ being the gliding and climbing Burger's vector densities for the distributed dislocations, respectively. The stress field in the absence of the crack is opposite equal to that generated by these distributed dislocations:

$$\sigma_{\hat{y}\hat{y}}(\hat{x})=-\frac{2\mu}{\pi(\kappa+1)}\int_{-a}^{+a}\left[B_{\hat{x}}(\hat{\xi})G_{\hat{x}\hat{y}\hat{y}}(\hat{x},0;\hat{\xi})+B_{\hat{y}}(\hat{\xi})G_{\hat{y}\hat{y}\hat{y}}(\hat{x},0;\hat{\xi})\right]\mathrm{d}\hat{\xi}, \tag{10a}$$

$$\sigma_{\hat{x}\hat{y}}(\hat{x})=-\frac{2\mu}{\pi(\kappa+1)}\int_{-a}^{+a}\left[B_{\hat{x}}(\hat{\xi})G_{\hat{x}\hat{x}\hat{y}}(\hat{x},0;\hat{\xi})+B_{\hat{y}}(\hat{\xi})G_{\hat{y}\hat{x}\hat{y}}(\hat{x},0;\hat{\xi})\right]\mathrm{d}\hat{\xi}. \tag{10b}$$

In our analysis, the crack is purely dislocation loaded, without exterior stress loading. It is worth to note that if exterior loading exists, it can be simply superposed into the formulation. As a result, for the current case, the boundary conditions in the local coordinate system are:

In the far field,

$$\sigma_{\hat{x}\hat{y}}=0,\quad \sigma_{\hat{y}\hat{y}}=0. \tag{11a}$$

Along the crack line,

$$\sigma_{\hat{x}\hat{y}}=0,\quad \sigma_{\hat{y}\hat{y}}=0,\quad d-a\leqslant\hat{x}\leqslant d+a; \tag{11b}$$

$$\lfloor\sigma_{\hat{x}\hat{y}}\rfloor=0,\quad \lfloor\sigma_{\hat{y}\hat{y}}\rfloor=0,\quad \hat{x}<d-a \text{ or } \hat{x}>d+a. \tag{11c}$$

where $[f]$ is the jump of the function f. Accordingly Eqs. (10a) and (10b) are re-written as

$$\int_{-a}^{+a}\left[B_{\hat{x}}(\hat{\xi})G_{\hat{x}\hat{y}\hat{y}}(\hat{x};\hat{\xi})+B_{\hat{y}}(\hat{\xi})G_{\hat{y}\hat{y}\hat{y}}(\hat{x};\hat{\xi})\right]\mathrm{d}\hat{\xi}=0, \tag{12a}$$

$$\int_{-a}^{+a}\left[B_{\hat{x}}(\hat{\xi})G_{\hat{x}\hat{x}\hat{y}}(\hat{x};\hat{\xi})+B_{\hat{y}}(\hat{\xi})G_{\hat{y}\hat{x}\hat{y}}(\hat{x};\hat{\xi})\right]\mathrm{d}\hat{\xi}=0. \tag{12b}$$

The microcrack should also satisfy the following two integral equations:

$$\int_{-a}^{+a} B_{\hat{x}}(\hat{\xi})\,\mathrm{d}\hat{\xi} = b_{\hat{x}}^{\mathrm{T}}, \tag{13a}$$

$$\int_{-a}^{+a} B_{\hat{y}}(\hat{\xi})\,\mathrm{d}\hat{\xi} = b_{\hat{y}}^{\mathrm{T}}, \tag{13b}$$

where $b_{\hat{x}}^{\mathrm{T}}$ and $b_{\hat{y}}^{\mathrm{T}}$ are the net dislocations inside the crack.

4. Solution procedure of the integral equations

To normalize the integral interval from $(-a,+a)$ to $(-1,+1)$ in the integral, we introduce

$$s = \hat{\xi}/a, \qquad t = \hat{x}/a. \tag{14}$$

Eqs. (12a) and (12b) are then rewritten in terms of s and t as

$$\int_{-1}^{+1} [B_{\hat{x}}(s)G_{\hat{x}\hat{y}\hat{y}}(t;s) + B_{\hat{y}}(s)G_{\hat{y}\hat{y}\hat{y}}(t;s)]\,\mathrm{d}s = 0, \tag{15a}$$

$$\int_{-1}^{+1} [B_{\hat{x}}(s)G_{\hat{x}\hat{x}\hat{y}}(t;s) + B_{\hat{y}}(s)G_{\hat{y}\hat{x}\hat{y}}(t;s)]\,\mathrm{d}s = 0. \tag{15b}$$

Since $B_{\hat{x}}(s)$ and $B_{\hat{y}}(s)$ are both singular at the two crack tips, solutions for them take the forms

$$B_{\hat{x}}(s) = \frac{D(s)}{(1-s^2)^{1/2}}, \tag{16a}$$

$$B_{\hat{y}}(s) = \frac{F(s)}{(1-s^2)^{1/2}}, \tag{16b}$$

where $D(s)$ and $F(s)$ are unknown functions to be evaluated. Eqs. (13a) and (13b) are similarly rewritten as

$$\int_{-1}^{+1} B_{\hat{x}}(s)\,\mathrm{d}s = \frac{b_{\hat{x}}^{\mathrm{T}}}{a} \tag{17a}$$

$$\int_{-1}^{+1} B_{\hat{y}}(s)\,\mathrm{d}s = \frac{b_{\hat{y}}^{\mathrm{T}}}{a}. \tag{17b}$$

Following the method developed by Erdogan and Gupta (1972) and Nowell and Hills (1987), the discretized forms of (15a), (15b), (17a) and (17b) are:

$$\frac{1}{N}\sum_{i=1}^{N}[G_{\hat{x}\hat{y}\hat{y}}(t_k,s_i)D(s_i) + G_{\hat{y}\hat{y}\hat{y}}(t_k,s_i)F(s_i)] = 0, \quad k = 1,\ldots,N-1, \tag{18a}$$

$$\frac{1}{N}\sum_{i=1}^{N}[G_{\hat{x}\hat{x}\hat{y}}(t_k,s_i)D(s_i) + G_{\hat{y}\hat{x}\hat{y}}(t_k,s_i)F(s_i)] = 0, \quad k = 1,\ldots,N-1, \tag{18b}$$

$$\frac{\pi}{N}\sum_{i=1}^{N}F(s_i) = \frac{b_{\hat{y}}^{\mathrm{T}}}{a}, \tag{18c}$$

$$\frac{\pi}{N}\sum_{i=1}^{N} D(s_i) = \frac{b_{\hat{x}}^{\mathrm{T}}}{a} \tag{18d}$$

with

$$s_i = \cos\left(\pi\frac{2i-1}{2N}\right), \quad i = 1,\ldots,N, \tag{18e}$$

$$t_k = \cos\left(\pi\frac{k}{N}\right), \quad k = 1,\ldots,N-1. \tag{18f}$$

Eqs. (18a)–(18d) altogether provide $2N$ linear algebraic equations to determine the $2N$ unknown values $D(s_i)$ and $F(s_i)$. Once these values are obtained, the dislocation density functions can be Eqs. (16a) and (16b). As a Zener–Stroh crack always propagates from the sharp tip (Xiao et al., 2000), only SIFs of the sharp tip are considered here. Once the dislocation density functions are obtained, the Mode I and Mode II SIFs at the sharp crack tip are given by (Weertman, 1996)

$$K_{\mathrm{I}} = \lim_{s\to 1}\frac{2\mu\sqrt{2\pi}}{\kappa+1}\sqrt{a(1-s)}B_{\hat{y}}(s) = -\frac{2\mu b_{\hat{y}}^{\mathrm{T}}\sqrt{\pi a}}{(\kappa+1)}F(1), \tag{19a}$$

$$K_{\mathrm{II}} = \lim_{s\to 1}\frac{2\mu\sqrt{2\pi}}{\kappa+1}\sqrt{a(1-s)}B_{\hat{x}}(s) = -\frac{2\mu b_{\hat{x}}^{\mathrm{T}}\sqrt{\pi a}}{(\kappa+1)}D(1). \tag{19b}$$

The value $F(1)$ and $D(1)$ are evaluated with Krenk interpolation formula (Krenk, 1975),

$$F(1) = \frac{1}{N}\sum_{i=1}^{N} F(s_i)\sin\left[\frac{2N-1}{4N}(2i-1)\pi\right]\Big/\sin\left(\frac{2i-1}{4N}\pi\right), \tag{20a}$$

$$F(1) = \frac{1}{N}\sum_{i=1}^{N} D(s_i)\sin\left[\frac{2N-1}{4N}(2i-1)\pi\right]\Big/\sin\left(\frac{2i-1}{4N}\pi\right). \tag{20b}$$

To find out the critical crack length a_{cr} at a given depth d, the following equation:

$$K_{\mathrm{I}}^2 + K_{\mathrm{II}}^2 = K_{\mathrm{IC}}^2 + K_{\mathrm{IIC}}^2 \tag{21}$$

is used based on energy consideration.

5. Numerical examples and discussion

In order to have a more direct understanding on the influences of different parameters on the fracture toughness of the crack, numerical calculations for various configurations have been performed. Figs. 4–7 show the variations of the SIFs at the sharp crack tip and the critical crack length with the slant angle θ and the crack depth d, respectively. In these calculations the shear and normal displacement loading selected for the analysis are equal ($b_{\hat{x}}^{\mathrm{T}} = b_{\hat{y}}^{\mathrm{T}}$). And the calculated SIFs and critical crack lengths are normalized by those of the same size crack in an isotropic infinite plane under the same loading, respectively.

In Fig. 4, the effect of the slant angle θ on the Mode I and Mode II SIFs of a Z-S crack is depicted. In this example the depth of the crack is taken as $d = 1.1a$, i.e., the crack is very near to the free surface of the material. It is observed that both the Mode I and Mode II SIFs increase from values lower than that in infinite plane to values higher than that in infinite plane, when the slant angle changes from 0 to π. For the two slant angles $\theta = 0$ and π, the crack is normal to the free surface. At this time we find the Mode I and

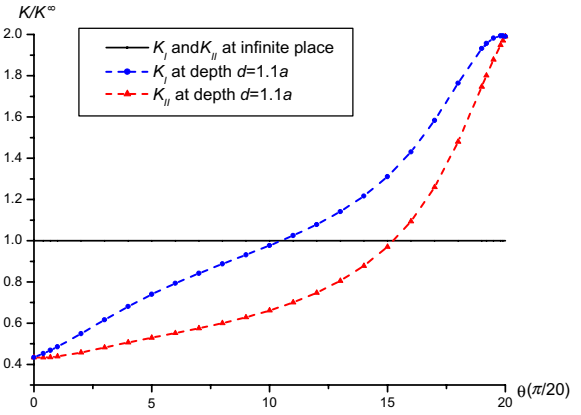

Fig. 4. The SIFs of the crack with $d = 1.1a$ as a function of the slant angle θ.

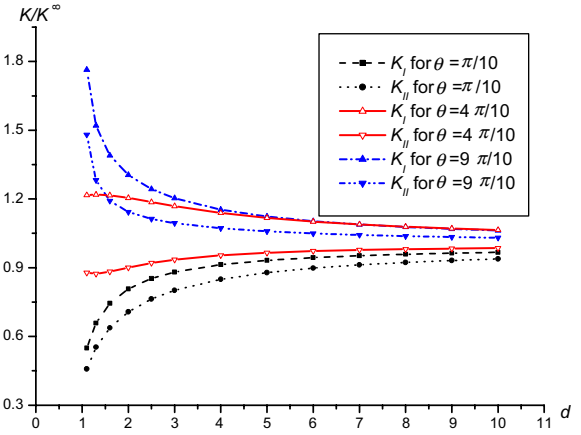

Fig. 5. The SIFs of the crack as a function of the depth d with the slant angle $\theta = \pi/10$, $4\pi/10$ and $9\pi/10$, respectively.

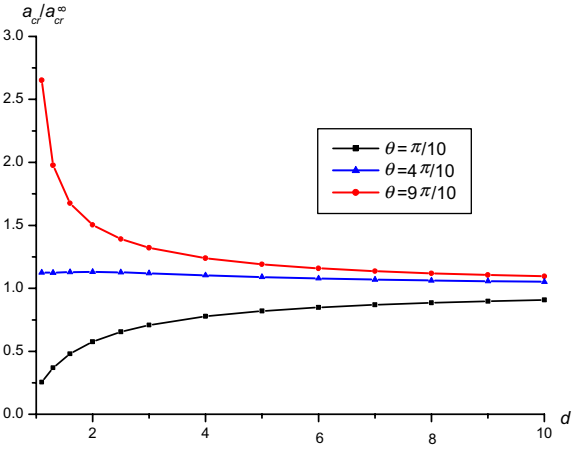

Fig. 6. Critical crack length as a function of the depth d with the slant angle $\theta = \pi/10$, $4\pi/10$ and $9\pi/10$, respectively.

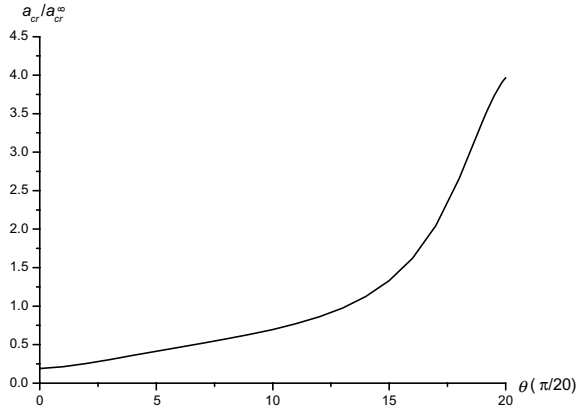

Fig. 7. Critical crack length as a function of the slant angle θ for $d = 1.1a$.

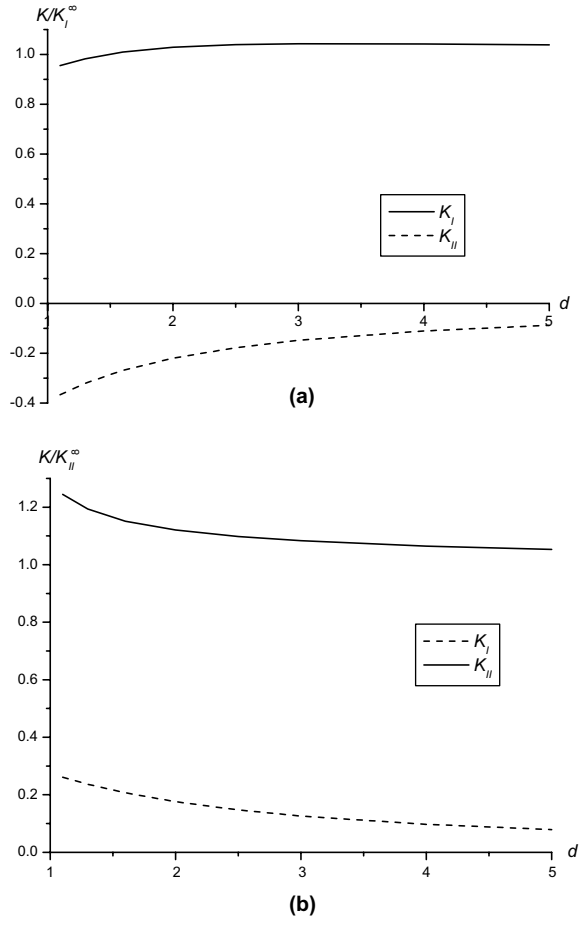

Fig. 8. The SIFs as a function of the depth d for $\theta = 7\pi/10$: (a) caused by Mode I displacement loading; (b) caused by Mode II displacement loading.

Mode II SIFs have the same value. This is because that at this condition, Eqs. (18a)–(18d) can be separated into two sets of independent equations, the two fracture modes are completely decoupled. In other words, Mode I loading will not cause any Mode II SIF, and the vice versa. The same phenomenon was also found for a subsurface Griffith crack (Nowell and Hills, 1987). For other θ value, the crack inclines to the surface, the Mode I and Mode II SIFs are coupled each other, because of the influence from the surface.

The influence of the crack depth d on the SIFs is illustrated in Fig. 5, for two different slant angles $\pi/10$, $\pi/10$ and $9\pi/10$. It is found that with the increasing depth, the SIFs approach their corresponding values in an infinite plane. This trend is understandable as the depth increases, the effect of the free surface decreases. Also it is observed that when d is small, the SIFs changes drastically with the depth d. It means the influence of the free surface on the crack is very strong when the crack is near to the surface. The current variation trend of the SIFs totally agrees with the study by Fan and Xiao (1997) for a Mode III Z-S crack, given as a by-product of a Mode III Zener–Stroh crack near an interface.

The relation between the critical crack length and the depth d is plotted in Fig. 6. The slant angle θ is chosen as $\pi/10$, $4\pi/10$ and $9\pi/10$, respectively. Because the critical crack length is determined by the energy release rate, which relates to the square of SIFs, the trend is similar to that given in the previous figure for the SIFs: the values approach to that in an infinite plane when the depth d increases. The variation of the critical crack length with the slant angle is illustrated in Fig. 7. It can be seen that when the slant angle

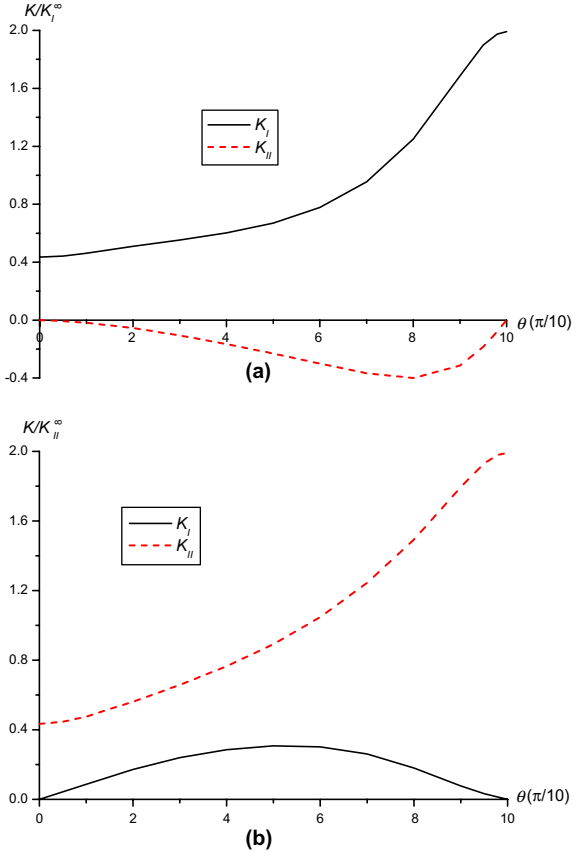

Fig. 9. The SIFs as a function of the slant angle θ for $d = 1.1a$: (a) caused by pure Mode I displacement loading; (b) caused by pure Mode II displacement loading.

increase form 0 to π, the critical crack length increase by a wide range: from less than half of that in an infinite plane to several times larger than that in an infinite plane. This is due to the fact that a Z-S crack propagates from the sharp crack tip only. For $\theta = 0$, the sharp tip is pointing away from the free surface; while for $\theta = \pi$, the sharp tip is towards to the surface.

In order to study the coupling effect between the two fracture modes, displacement loading selected for the calculations in Figs. 8 and 9 is either pure net climbing dislocations $b_{\hat{y}}^{\mathrm{T}}$ (corresponding to pure normal stress loading), or gliding dislocations $b_{\hat{x}}^{\mathrm{T}}$ (corresponding to pure shear stress loading). Fig. 8 shows that a single mode type of loading generates both Mode I and Mode II SIFs for the Z-S crack with a slant angle $7\pi/10$, which is totally different to that in an infinite plane. With the increasing depth d, the Mode II SIF induced by the Mode I loading or the Mode I SIF induced by the Mode II loading will decrease and finally disappear. The variation of the SIFs with the slant angle is plotted in Fig. 9, for either pure $b_{\hat{y}}^{\mathrm{T}}$ loading or pure $b_{\hat{x}}^{\mathrm{T}}$ loading, respectively. When the crack is normal to the free surface, the two fracture modes are decoupled completely.

6. Conclusion

A subsurface Zener–Stroh crack has been investigated from its nucleation to fracture behavior after its initiation. In nucleation procedure, the equilibrium equation of the force on dislocations is given. When the crack is nucleated, the influences of the free surface and the slant angle on the crack have been studied in detail. It is found that when the crack is near to the free surface, the effect of the surface on the fracture behavior is very large. Since a Z-S crack propagates from its sharp crack tip only, the slant angle plays a key role on the SIFs and the critical crack length. Another physical feature is that the Mode I and Mode II SIFs of the crack are intrinsically coupled each other, as long as the crack is not normal to the free surface.

Appendix A. The influence function and transformation in two coordinate systems

The influence function due to a single dislocation in half plane was cleared up by Hills et al. (1996),

$$G_{xxx} = (y-\eta)\left(-\frac{1}{r_1^2} - \frac{2x_1^2}{r_1^4} + \frac{1}{r_2^2} - \frac{2x_2^2}{r_2^4} - \frac{4\xi x_2}{r_2^4} + \frac{4\xi^2}{r_2^4} + \frac{16\xi x_2^3}{r_2^6} - \frac{16\xi^2 x_2^2}{r_2^6} \right), \tag{A.1}$$

$$G_{yxx} = -\frac{x_1}{r_1^2} + \frac{2x_1^3}{r_1^4} + \frac{x_2}{r_2^2} - \frac{2\xi}{r_2^2} - \frac{2x_2^3}{r_2^4} - \frac{8\xi x_2^2}{r_2^4} + \frac{12\xi^2 x_2}{r_2^4} + \frac{16\xi x_2^4}{r_2^6} - \frac{16\xi^2 x_2^3}{r_2^6}, \tag{A.2}$$

$$G_{xyy} = (y-\eta)\left(-\frac{1}{r_1^2} + \frac{2x_1^2}{r_1^4} + \frac{1}{r_2^2} - \frac{2x_2^2}{r_2^4} + \frac{12\xi x_2}{r_2^4} - \frac{4\xi^2}{r_2^4} - \frac{16\xi x_2^3}{r_2^6} + \frac{16\xi^2 x_2^2}{r_2^6} \right), \tag{A.3}$$

$$G_{yyy} = \frac{3x_1}{r_1^2} - \frac{2x_1^3}{r_1^4} - \frac{3x_2}{r_2^2} - \frac{2\xi}{r_2^2} + \frac{2x_2^3}{r_2^4} + \frac{16\xi x_2^2}{r_2^4} - \frac{12\xi^2 x_2}{r_2^4} - \frac{16\xi x_2^4}{r_2^6} + \frac{16\xi^2 x_2^3}{r_2^6}, \tag{A.4}$$

$$G_{xxy} = -\frac{x_1}{r_1^2} + \frac{2x_1^3}{r_1^4} + \frac{x_2}{r_2^2} - \frac{2\xi}{r_2^2} - \frac{2x_2^3}{r_2^4} + \frac{16\xi x_2^2}{r_2^4} - \frac{12\xi^2 x_2}{r_2^4} - \frac{16\xi x_2^4}{r_2^6} + \frac{16\xi^2 x_2^3}{r_2^6}, \tag{A.5}$$

$$G_{yxy} = (y-\eta)\left(-\frac{1}{r_1^2} + \frac{2x_1^2}{r_1^4} + \frac{1}{r_2^2} - \frac{2x_2^2}{r_2^4} - \frac{4\xi x_2}{r_2^4} + \frac{4\xi^2}{r_2^4} + \frac{16\xi x_2^3}{r_2^6} - \frac{16\xi^2 x_2^2}{r_2^6} \right), \tag{A.6}$$

where

$$x_1 = x - \xi, \quad x_2 = x + \xi, \tag{A.7}$$

$$r_1^2 = (x-\xi)^2 + (y-\eta)^2, \quad r_2^2 = (x+\xi)^2 + (y-\eta)^2. \tag{A.8}$$

The transformation from the global coordinate system x–y to the local coordinate system $\hat{x}$–$\hat{y}$ can be performed in two steps. Firstly, we express the stress field in global coordinate system with the position expressed in local coordinate system, viz., $\sigma_{ij}(\hat{x},\hat{y})$. The mathematical relations between these two systems are

$$\begin{cases} x = \hat{x}\cos\theta + d, \\ y = \hat{x}\sin\theta, \\ \xi = \hat{\xi}\cos\theta + d, \\ \eta = \hat{\xi}\sin\theta. \end{cases} \tag{A.9}$$

Then we calculate the shear and normal stresses in the local system with Mohr's circle, viz., $\sigma_{\hat{i}\hat{j}}(\hat{x},\hat{y})$, and change the Burger's vectors expressed in local systems.

The transformation of the influence function is

$$\begin{bmatrix} \sigma_{\hat{x}\hat{x}}(\hat{x},\hat{y}) \\ \sigma_{\hat{y}\hat{y}}(\hat{x},\hat{y}) \\ \sigma_{\hat{x}\hat{y}}(\hat{x},\hat{y}) \end{bmatrix} = \begin{bmatrix} \cos^2\theta & \sin^2\theta & \sin 2\theta \\ \sin^2\theta & \cos^2\theta & -\sin 2\theta \\ -\sin\theta\cos\theta & \sin\theta\cos\theta & \cos 2\theta \end{bmatrix} \begin{bmatrix} \sigma_{xx}(\hat{x},\hat{y}) \\ \sigma_{yy}(\hat{x},\hat{y}) \\ \sigma_{xy}(\hat{x},\hat{y}) \end{bmatrix}. \tag{A.10}$$

The transformation of Burgers vectors is

$$\begin{Bmatrix} b_x \\ b_y \end{Bmatrix} = \begin{bmatrix} \cos\theta & -\sin\theta \\ \sin\theta & \cos\theta \end{bmatrix} \begin{Bmatrix} b_{\hat{x}} \\ b_{\hat{y}} \end{Bmatrix}. \tag{A.11}$$

Finally, the stress field in the new local coordinate system is written as

$$\begin{Bmatrix} \sigma_{\hat{y}\hat{y}}(\hat{x},\hat{y}) \\ \sigma_{\hat{y}\hat{y}}(\hat{x},\hat{y}) \end{Bmatrix} = \frac{2\mu}{\pi(\kappa+1)} \begin{bmatrix} G_{\hat{x}\hat{y}\hat{y}}(\hat{x},\hat{y};\hat{\xi}) & G_{\hat{y}\hat{y}\hat{y}}(\hat{x},\hat{y};\hat{\xi}) \\ G_{\hat{x}\hat{x}\hat{y}}(\hat{x},\hat{y};\hat{\xi}) & G_{\hat{y}\hat{x}\hat{y}}(\hat{x},\hat{y};\hat{\xi}) \end{bmatrix} \begin{Bmatrix} b_{\hat{x}}(\hat{\xi}) \\ b_{\hat{y}}(\hat{\xi}) \end{Bmatrix}. \tag{A.12}$$

References

Bower, A.F., 1988. The influence of crack face friction and trapped fluid on surface initiated rolling contact fatigue cracks. ASME Journal of Tribology 110, 704–711.

Cherepanov, G.P., 1994. Interface microcrack nucleation. Journal of the Mechanics and Physics of Solids 42, 665–680.

Cottrell, A.H., 1958. Theory of brittle fracture in steel and similar metals. Transaction of the Metallurgical Society of the AIME 212, 192–203.

Dundurs, J., 1969. Elastic interaction of dislocations with inhomogeneities. In: Mura, T. (Ed.), The Mathematical Theory of Dislocations. ASME, New York, pp. 70–115.

Erdogan, F., Gupta, G.D., 1972. On the numerical solution of singular integral equations. Quarterly of Applied Mathematics 30, 525–534.

Fan, H., 1994. Interfacial Zener–Stroh crack. Journal of Applied Mechanics 61, 829–834.

Fan, H., Xiao, Z.M., 1997. A Zener–Stroh crack near an interface. International Journal of Solids and Structures 34, 2829–2842.

Hearle, A.D., Johnson, K.L., 1985. Mode II SIFs for a crack parallel to the surface of an elastic half-space subjected to a moving point load. Journal of the Mechanics and Physics of Solids 33, 61–81.

Hills, D.A., Comninou, M., 1985. A normally loaded half plane with an edge crack. International Journal of Solids and Structures 21, 399–410.

Hills, D.A., Kelly, P.A., Dai, D.N., Korsunsky, A.M., 1996. Solution of Crack Problems, The Distributed Dislocation Technique. Kluwer Academic Publishers.

Hsia, K.J., Xu, Z.-Q., 1996. The mathematical framework and an approximate solution of surface crack propagation under hydraulic pressure loading. International Journal of Fracture 78, 363–378.

Kikuchi, M., Shiozawa, K., Weertman, J.R., 1981. Void nucleation in astrology: theory and experiments. Acta Metallurgica 29, 1747–1758.

Krenk, S., 1975. On the use of the interpolation polynomial for solutions of singular integral equations. Quart. Appl. Math. 32, 479–484.

Minowa, K., Sumino, K., 1992. Stress-induced amorphization of a silicon crystal by mechanical scratching. Physics Review Letter 69, 320–322.

Nowell, D., Hills, D.A., 1987. Open cracks at or near free edges. Journal of Strain Analysis 22, 177–185.

Stroh, A.N., 1954. The formation of cracks as a result of plastic flow, I. Proceedings of The Royal Society of London Series, A 223, 404–414.

Stroh, A.N., 1955. The formation of cracks as a result of plastic flow, II. Proceedings of The Royal Society of London Series, A 232, 548–560.

Weertman, J.R., 1986. Zener–Stroh crack, Zener–Hollomon parameter, and other topics. Journal of Applied Physics 60, 1877–1887.

Weertman, J., 1996. Dislocation Based Fracture Mechanics. World Scientific, Singapore.

Xiao, Z.M., Fan, H., 1996. Microcrack initiation at tip of a rigid line inhomogeneity. International Journal of Fracture 82, 1–9.

Xiao, Z.M., Chen, B.J., Fan, H., 2000. A Zener–Stroh crack in a fiber-reinforced composite material. Mechanics of Materials 32, 593–606.

Xu, Z.-Q., Hsia, K.J., 1997. A numerical solution of surface crack under cyclic hydraulic pressure loading. ASME Journal of Tribology 119, 637–645.

Zener, C., 1948. The micro-mechanism of fracture. In: Fracturing of Metals. American Society of Metals, Cleveland, pp. 3–31.

Zhang, B., Zheng, X.L., Tokura, H., Yoshikawa, M., 2003. Grinding induced damage in ceramics. Journal of Material Processing Technology 132, 353–364.